Total Variation-Penalized Poisson Likelihood Estimation for Ill-Posed Problems

Johnathan M. Bardsley† ‡

Department of Mathematical Sciences, University of Montana, Missoula, MT.
Email: bardsleyj@mso.umt.edu

Aaron Luttman

Division of Science and Mathematics, Bethany Lutheran College, Mankato, MN.
Email: luttman@blc.edu

Abstract. The noise contained in data measured by imaging instruments is often primarily of Poisson type. This motivates, in many cases, the use of the Poisson likelihood functional in place of the ubiquitous least squares data fidelity when solving image deblurring problems. We assume that the underlying blurring operator is compact, so that, as in the least squares case, the resulting minimization problem is ill-posed and must be regularized. In this paper, we focus on total variation regularization and show that the problem of computing the minimizer of the resulting total variation-penalized Poisson likelihood functional is well-posed. We then prove that, as the errors in the data and in the blurring operator tend to zero, the resulting minimizers converge to the minimizer of the exact likelihood function. Finally, the practical effectiveness of the approach is demonstrated on synthetically generated data, and a nonnegatively constrained, projected quasi-Newton method is introduced.

PACS numbers: 02.30.Zz, 02.50.-r, 07.05.Pj

Keywords: total variation regularization, ill-posed problems, maximum likelihood estimation, image deblurring, nonnegatively constrained minimization.

1. Introduction

We consider equations of the type

$$Au = z, \tag{1}$$

† To whom correspondence should be addressed.
‡ This work was supported by the NSF under grant DMS-0504325. It was completed during the author's visit to the University of Helsinki, Finland in 2006-07 under the University of Montana Faculty Exchange Program.

where A is a linear operator from $L^p(\Omega)$ to $L^2(\Omega)$. In a wide range of applications, e.g., astronomical and biological imaging, A is a compact operator of Fredholm first kind

$$Au(x) = \int_\Omega k(x,y)u(y)\,dy. \tag{2}$$

In such cases, (1) is an ill-posed problem [10, 11]. Because of this, (pseudo) solutions of (1) are typically unstable with respect to perturbations in A and z, so the problem must be regularized. Perhaps the most standard regularization approach, due to Tikhonov, is to solve the variational problem

$$\min_u \|Au - z\|_2^2 + \alpha J(u)^2, \tag{3}$$

where α is known as the *regularization parameter*, and J is a problem-dependent penalty functional that provides stability and incorporates prior knowledge about the true solution. If the true solution is known to have jump discontinuities, a natural choice for J [1, 12] is

$$J(u) = J_\beta(u) \stackrel{\text{def}}{=} \int_\Omega \sqrt{|\nabla u|^2 + \beta}\,dx, \tag{4}$$

where $\beta \geq 0$. For $\beta = 0$, (4) is known as the *total variation* of u.

In practical applications, the function z in (1) is a continuous representative of the discrete, collected data, which we will denote $\mathbf{z}$. In a variety of imaging applications, the data consists of a $n \times n$ array of intensity values measured by a charge coupled device (CCD) camera. The elements of this array can be column stacked, or lexicographically ordered, making $\mathbf{z}$ an $n^2 \times 1$ vector. A quadrature approximation of (2) then allows one to express (1) as a discrete linear system of the form

$$\mathbf{Au} = \mathbf{z}, \tag{5}$$

where $\mathbf{A} \in \mathbb{R}^{n^2 \times n^2}$ is known as the blurring matrix and $\mathbf{u} \in \mathbb{R}^{n^2}$ is unknown. The discrete analogue of (3), (4) is then given by

$$\min_{\mathbf{u}} \|\mathbf{Au} - \mathbf{z}\|_2^2 + \alpha J_\beta(\mathbf{u})^2, \tag{6}$$

where $J_\beta(\mathbf{u})$ is a numerical approximation of (4).

Solving (6) is the standard approach that is taken when total variation regularization is implemented computationally. This is due to the fact that a number of effective algorithms have been developed for its solution (see [11, Chapter 8] and the references therein). Furthermore, the theoretical analysis of the underlying continuous problem (3), (4) found in [1] puts the approach on firm theoretical footings.

However, for data $\mathbf{z}$ measured by a CCD camera, the least squares data fidelity in (6) is not optimal. To see this, note that CCD camera intensity measurements are stochastic, and hence, $\mathbf{z}$ is a realization of the random vector $\hat{\mathbf{z}}$, which takes the form (cf. [8, 9])

$$\hat{\mathbf{z}} \sim \text{Poiss}(\mathbf{Au}_{\text{true}}) + \text{Poiss}(\gamma \cdot \mathbf{1}) + N(\mathbf{0}, \sigma^2 I), \tag{7}$$

where $\mathbf{u}_{\text{true}}$ is the $n^2 \times 1$ discrete, column stacked, true image; $\mathbf{1}$ is an $n^2 \times 1$ vector of all ones; and I is the $n^2 \times n^2$ identity matrix. Equation (7) means that each element $\hat{z}_i$ of the vector $\hat{\mathbf{z}}$ is a random variable with distribution

$$\hat{z}_i \sim \mathrm{n}_{\text{obj}}(i) + \mathrm{n}_0(i) + g(i), \quad i = 1, \ldots, n^2, \tag{8}$$

where

- $\mathrm{n}_{\text{obj}}(i)$ is the number of object dependent photoelectrons measured by the ith detector in the CCD array. It is a Poisson random variable with Poisson parameter $[\mathbf{A}\mathbf{u}_{\text{true}}]_i$.
- $\mathrm{n}_0(i)$ is the number of background photoelectrons, which arise from both natural and artificial sources, measured by the ith detector in the CCD array. It is a Poisson random variable with a fixed positive Poisson parameter γ.
- $g(i)$ is the so-called readout noise, which is due to random errors caused by the CCD electronics and errors in the analog-to-digital conversion of measured voltages. It is a Gaussian random variable with mean 0 and fixed variance σ^2.

The random variables $\mathrm{n}_{\text{obj}}(i)$, $\mathrm{n}_0(i)$, and $g(i)$ are assumed to be independent of one another and of $\mathrm{n}_{\text{obj}}(j)$, $\mathrm{n}_0(j)$, and $g(j)$ for $i \neq j$. As in [8], we consider the case in which the readout noise variance σ^2 is large. Then, according to Feller [5, pp. 190 and 245], the following approximation is accurate:

$$N(\sigma^2, \sigma^2) \approx \text{Poiss}(\sigma^2). \tag{9}$$

Using this approximation and the independence properties of the random variables in (8) we obtain the following approximation of (7):

$$\hat{\mathbf{z}} + \sigma^2 \cdot \mathbf{1} \sim \text{Poiss}(\mathbf{A}\mathbf{u}_{\text{true}} + \gamma \cdot \mathbf{1} + \sigma^2 \cdot \mathbf{1}). \tag{10}$$

The maximum likelihood estimate of $\mathbf{u}_{\text{true}}$ given statistical model (10) is the minimizer with respect to $\mathbf{u}$ of the Poisson likelihood functional

$$T_0(\mathbf{u}) \stackrel{\text{def}}{=} \sum_{i=1}^{N}([\mathbf{A}\mathbf{u}]_i + \gamma + \sigma^2) - \sum_{i=1}^{N}(z_i + \sigma^2)\log([\mathbf{A}\mathbf{u}]_i + \gamma + \sigma^2). \tag{11}$$

Thus for data $\mathbf{z}$ collected by a CCD camera, T_0 is a more appropriate choice of fit-to-data function than is the least squares functional.

As with the least squares likelihood, since $\mathbf{A}$ is ill-conditioned, regularization is required. If (11) is regularized with the total variation functional and the associated minimization problem is component-wise nonnegatively constrained - incorporating the prior knowledge that the true image, in fact, satisfies this constraint - we obtain the constrained variational problem

$$\min_{\mathbf{u} \geq \mathbf{0}} T_\alpha(\mathbf{u}) \stackrel{\text{def}}{=} T_0(\mathbf{u}) + \alpha J_\beta(\mathbf{u}). \tag{12}$$

Problem (12) serves as the motivation for this paper. We will present a theoretical justification of this approach, as well as effective computational methods for its solution.

The theoretical analysis is performed on the continuous analogue of (12), which is given by

$$\min_{u\in\mathcal{C}} T_\alpha(u) \stackrel{\text{def}}{=} T_0(u) + \alpha J_\beta(u), \tag{13}$$

where

$$T_0(u) = \int_\Omega \left((Au+\gamma+\sigma^2) - (z+\sigma^2)\log(Au+\gamma+\sigma^2)\right)\, dx, \tag{14}$$

and

$$\mathcal{C} = \{u \in BV(\Omega) \mid u \geq 0 \text{ almost everywhere}\}. \tag{15}$$

Here Ω is a bounded and convex subset of $\mathbb{R}^d$ for $d = 1$, 2, 3 with Lipschitz continuous boundary; and

$$BV(\Omega) = \{u \in L^1(\Omega) : J_0(u) < \infty\}, \tag{16}$$

with J_0 defined by (4), is the space of functions of *bounded variation*. Note that the presence of $BV(\Omega)$ in (15) is a result of the fact that total variation regularization restricts possible solutions to this set. Also, although our motivating example is two-dimensional, we allow for Ω to be a subset of $\mathbb{R}^d$ for $d = 1$, 2 or 3 so that our analysis will be as general as possible.

In order to connect T_0 with an underlying operator equation of the form (1), we compute its gradient and Hessian, which are given, respectively, by

$$\nabla T_0(u) \ = A^*\left(\frac{Au-(z-\gamma)}{Au+\gamma+\sigma^2}\right), \tag{17}$$

$$\nabla^2 T_0(u) = A^*\left(\frac{z+\sigma^2}{(Au+\gamma+\sigma^2)^2}\right)A, \tag{18}$$

where "$*$" denotes operator adjoint. Provided $z+\sigma^2 > 0$ (a reasonable assumption in imaging applications), we see that (18) is a positive definite operator. Thus T_0 is strictly convex [11, Theorem 2.42], and hence, has a unique minimizer u_{exact} over $\mathcal{C}$. If $u_{\text{exact}} > 0$, then $\nabla T_0(u_{\text{exact}}) = 0$, or, equivalently,

$$Au_{\text{exact}} = z - \gamma. \tag{19}$$

Thus (13) can be viewed as a constrained and regularized variational formulation of the operator equation (19).

The goal of the theoretical analysis is to show that (13), (14) is a theoretically well-posed problem for all $\alpha > 0$, i.e. that (13) has a unique solution that is stable with respect to perturbations in z and A for all $\alpha > 0$, and that, as perturbations in the data z and the operator A disappear, the regularization parameter α can be chosen so that the corresponding solutions of (13) converge to the minimizer u_{exact} of the Poisson likelihood functional T_0 over $\mathcal{C}$. This was done in [1] for (3), (4).

Once the theoretical analysis of problem (13) is complete, we will discuss numerical methods for solving (12). We present two nonnegatively constrained minimization algorithms. The first is the well-known projected gradient method. Due to the

fact that the minimization problem is constrained, large-scale and ill-conditioned, a more robust method is required in order to obtain accurate approximations of the exact solution of (12), so we also present a nonnegatively constrained quasi-Newton method. The formulas for both the gradient and the Hessian of $T_\alpha(\mathbf{u})$ are needed in the implementation of these methods and are therefore presented as well.

The paper is organized as follows. In Section 2, we present our theoretical analysis of problem (13). We then demonstrate the practical effectiveness of total variation-penalized Poisson likelihood estimation with a numerical experiment in Section 3. We end with conclusions in Section 4.

2. Theoretical Analysis

In this section, we present a theoretical analysis of (13). In particular, we show that (13) is well-posed and that as errors in the data and in the operator disappear, the corresponding minimizers converge to the minimizer u_{exact} of T_0 over $\mathcal{C}$. We begin with some analytic preliminaries.

2.1. Analytic Preliminaries

Let Ω and $\mathcal{C}$ be as defined in the introduction. Then $|\Omega| = \int_\Omega dx < \infty$. We will assume that $Au \geq 0$ for every $u \in \mathcal{C}$, and that $z \in L^\infty(\Omega)$ with $z + \sigma^2 > 0$, which are reasonable assumptions on A and z for imaging applications.

Let $|\cdot|$ denote the Euclidean norm in $\mathbb{R}^d$ and $\|\cdot\|_p$ the Banach space norm on $L^p(\Omega)$ for $1 \leq p \leq \infty$. Since Ω is bounded, $L^p(\Omega) \subset L^1(\Omega)$, $p > 1$.

We now give a number of results and definitions regarding $BV(\Omega)$. First of all, $BV(\Omega)$ is a Banach space with respect to the norm

$$\|u\|_{BV} = \|u\|_1 + J_0(u).$$

J_0 is known as the *total variation* and defines a seminorm on $BV(\Omega)$. Since $\sqrt{x} \leq \sqrt{x+\beta} \leq \sqrt{x} + \sqrt{\beta}$ for $\beta, x \geq 0$, we have

$$J_0(u) \leq J_\beta(u) \leq J_0(u) + \sqrt{\beta}|\Omega|. \tag{20}$$

Inequality (20) will allow us to assume, without loss of generality, that $\beta = 0$ in several of our arguments.

A set $\mathcal{S} \subset BV(\Omega)$ is said to be *BV-bounded* if there exists $B > 0$ such that $\|u\|_{BV} \leq B$ for all $u \in \mathcal{S}$.

A functional $T : L^p(\Omega) \to \mathbb{R}$ is said to be *BV-coercive* if

$$T(u) \to +\infty \quad \text{whenever} \quad \|u\|_{BV} \to +\infty. \tag{21}$$

Note that by definition $BV(\Omega) \subset L^1(\Omega)$, and as a consequence of the following lemma [1], which will be useful in the sequel, $BV(\Omega) \subset L^p(\Omega)$ for $1 \leq p \leq d/(d-1)$, where for $d = 1$, $d/(d-1) \stackrel{\text{def}}{=} +\infty$.

Lemma 1. *Let $\mathcal{S}$ be a BV-bounded set of functions. Then $\mathcal{S}$ is relatively compact, i.e. its closure is compact, in $L^p(\Omega)$ for $1 \leq p < d/(d-1)$. $\mathcal{S}$ is bounded and thus relatively weakly compact for dimensions $d \geq 2$ in $L^p(\Omega)$ for $p = d/(d-1)$.*

2.2. Well-Posedness

We now prove that problem (13) is well-posed for $\alpha > 0$, i.e. that (13) has a unique solution, and that this solution is stable with respect to perturbations in z and A. We begin by showing that a solution of (13) exists and is unique.

2.2.1. Existence and Uniqueness of Solutions In order to prove the existence and uniqueness of solutions of (13), we will use the following theorem, which is similar to [1, Theorem 3.1].

Theorem 1. *If $T : L^p(\Omega) \to \mathbb{R}$ is strictly convex and BV-coercive, and $1 \leq p \leq d/(d-1)$, then T has a unique minimizer on $\mathcal{C}$.*

Proof. Let $\{u_n\} \subset \mathcal{C}$ be such that $T(u_n) \to \inf_{u \in \mathcal{C}} T(u)$. Then $T(u_n)$ is bounded, and hence, by (21), $\{u_n\}$ is BV-bounded. Lemma 1 implies that there exists a subsequence $\{u_{n_j}\}$ that converges to some $u_* \in L^p(\Omega)$. Convergence is weak if $p = d/(d-1)$. Since T is strictly convex, it is weakly lower semi-continuous [13], and hence,

$$T(u_*) \leq \liminf T(u_{n_j}) = \lim T(u_n) = T_*,$$

where T_* is the infimum of T on $\mathcal{C}$. Thus u_* minimizes T on $\mathcal{C}$ and is unique since T is a strictly convex functional and $\mathcal{C}$ is a convex set. □

In order to use Theorem 1, we must show that T_α (as defined in (13)) is both strictly convex and BV-coercive. This is done in the following two lemmas.

Lemma 2. *T_α is strictly convex.*

Proof. In the introduction we showed that T_0 is strictly convex. The strict convexity of T_α then follows immediately from the fact that J_β is convex, which is proved in [1]. □

Lemma 3. *T_α is BV-coercive on $\mathcal{C}$.*

Proof. By (21), we must show that if $\|u\|_{BV} \to \infty$, then $T_\alpha(u) \to \infty$. A straightforward computation yields the following decomposition of a function $u \in BV(\Omega)$:

$$u = v + w, \tag{22}$$

where

$$w = \left(\int_\Omega u \, dx \Big/ |\Omega| \right) \chi_\Omega, \quad \text{and} \quad \int_\Omega v \, dx = 0. \tag{23}$$

Here χ_Ω is the indicator function on Ω. It is shown in [1] that there exists $C_1 \in \mathbb{R}^+$ such that

$$\|v\|_p \leq C_1 J_0(v), \tag{24}$$

for $1 \leq p \leq d/(d-1)$. Equation (24), the triangle inequality, and the fact that $J_0(w) = 0$ yield

$$\|u\|_{BV} \leq \|w\|_1 + (C_1 + 1)J_0(v). \tag{25}$$

Thus if $\|u\|_{BV} \to \infty$, either $\|w\|_1 \to \infty$ or $J_0(v) \to \infty$.

Let u_{exact} be the unique minimizer of Poisson likelihood T_0 over $\mathcal{C}$. Then, since $T_\alpha(u) \geq T_0(u_{\text{exact}}) + \alpha J_0(v)$, we see that $J_0(v) \to \infty$ implies $T_\alpha(u) \to \infty$.

If $\|u\|_{BV} \to \infty$ and $J_0(v)$ is bounded, from (25) we have $\|w\|_1 \to \infty$. Noting that

$$\|Aw\|_1 = \left(\|A\chi_\Omega\|_1 / |\Omega|\right) \|w\|_1 = C_2\|w\|_1, \tag{26}$$

since $Au \geq 0$ for all $u \in \mathcal{C}$, Jensen's inequality together with (24) and (26) yields

$$\begin{aligned}
T_\alpha(u) &\geq \|Au + \gamma + \sigma^2\|_1 - \|z + \sigma^2\|_\infty \log \|Au + \gamma + \sigma^2\|_1, &(27)\\
&\geq \|Aw\|_1 - \|Av\|_1 - (\gamma + \sigma^2)|\Omega| \\
&\qquad - \|z + \sigma^2\|_\infty \log\left(\|Aw\|_1 + \|Av\|_1 + (\gamma + \sigma^2)|\Omega|\right), \\
&\geq C_2\|w\|_1 - \|A\|_1 C_1 J_0(v) - (\gamma + \sigma^2)|\Omega| \\
&\qquad - \|z + \sigma^2\|_\infty \log\left(C_2\|w\|_1 + \|A\|_1 C_1 J_0(v) + (\gamma + \sigma^2)|\Omega|\right), \\
&\geq C_2\|w\|_1 - M - \|z + \sigma^2\|_\infty \log(C_2\|w\|_1 + M), &(28)
\end{aligned}$$

where M is the upper bound of $\|A\|_1 C_1 J_0(v) + (\gamma + \sigma^2)|\Omega|$, and $\|A\|_1$ is the operator norm induced by the norm on $L^1(\Omega)$. From (28), we see that $T_\alpha(u) \to \infty$ if $\|w\|_1 \to \infty$, which completes the proof. □

An appeal to Lemmas 2 and 3 immediately yields the following corollary of Theorem 1.

Corollary 1 (Existence and Uniqueness of Minimizers)**.** *T_α has a unique minimizer over $\mathcal{C}$.*

Before continuing, we note that in the denoising case, i.e. when A is the identity operator, the existence and uniqueness of minimizers of $T_\alpha(u)$ was proved in [2].

2.2.2. Stability of Solutions In order to prove stability of minimizers of (13) with respect to perturbations in A and z, we consider the sequence of perturbed variational problems

$$\min_{u \in \mathcal{C}} T_{\alpha,n}(u) \stackrel{\text{def}}{=} \int_\Omega \left((A_n u + \gamma + \sigma^2) - (z_n + \sigma^2)\log(A_n u + \gamma + \sigma^2)\right) dx + \alpha J_\beta(u), \tag{29}$$

where $A_n u \geq 0$ for all $n \in \mathbb{N}$ and all $u \in \mathcal{C}$ and $z_n > \sigma^2$ for all $n \in \mathbb{N}$. By the above analysis, $T_{\alpha,n}$ is then strictly convex, BV-coercive, and has a unique solution in $\mathcal{C}$ for all n. Minimizers of (13) are then stable provided that as $A_n \to A$ and $z_n \to z$, the minimizers of the $T_{\alpha,n}$'s over $\mathcal{C}$ converge to the minimizer of T_α over $\mathcal{C}$.

The following theorem (from [1]) gives conditions on the $T_{\alpha,n}$'s that guarantee that (13) is stable.

Theorem 2. *Assume that $1 \leq p \leq d/(d-1)$ and that T_α and each of the $T_{\alpha,n}$'s are BV-coercive, lower semicontinuous and have a unique minimizer. Assume in addition*

(i) Uniform BV-coercivity: For any sequence $\{u_n\} \subset L^p(\Omega)$,

$$\lim T_{\alpha,n}(u_n) = +\infty \quad \textit{whenever} \quad \lim \|u_n\|_{BV} = +\infty. \tag{30}$$

(ii) Consistency: $T_{\alpha,n} \to T_\alpha$ uniformly on BV-bounded sets, i.e., given $B > 0$ and $\epsilon > 0$, there exists N such that

$$|T_{\alpha,n}(u) - T_\alpha(u)| < \epsilon \quad \textit{whenever} \quad n \geq N,\ \|u\|_{BV} \leq B. \tag{31}$$

Then problem (13) is stable with respect to the perturbations (29), i.e. if u_* minimizes T_α and u_n minimizes $T_{\alpha,n}$, then

$$\|u_n - u_*\|_p \to 0.$$

If $p = d/(d-1)$, $d \geq 2$, and T_α and each $T_{\alpha,n}$ are weakly lower semicontinuous, then convergence is weak:

$$u_n - u \rightharpoonup 0.$$

The following corollary of Theorem 2 then yields the stability result for (13) that we seek.

Corollary 2 (Stability of Minimizers)**.** *Assume $1 \leq p < d/(d-1)$, $\|z_n - z\|_\infty \to 0$, and that the A_n's are bounded linear and converge pointwise to A in $L^p(\Omega)$. Also assume that T_α and $T_{\alpha,n}$ as defined by (13) and (29), respectively, have unique minimizers u_* and u_n. Then*

$$\|u_n - u_*\|_p \to 0.$$

If $p = d/(d-1)$, convergence is weak.

Proof. Without loss of generality, due to (20), we focus on the $\beta = 0$ case and show that conditions 1 and 2 from Theorem 2 hold.

For condition 1, we repeat the proof of Lemma 3. Taking $u_n = v_n + w_n$, we know that if $\|u_n\|_{BV} \to \infty$, either $J_0(v_n) \to \infty$ or $\|w_n\|_1 \to \infty$.

First, since $T_{\alpha,n}(u_n) \geq T_{0,n}(u_{n*}) + \alpha J_0(v_n)$, where u_{n*} is the unique minimizer of $T_{0,n}$, we see that if $T_{0,n}(u_{n*})$ is bounded below, $J_0(v_n) \to \infty$ implies $T_\alpha(u_n) \to \infty$. To see that $T_{0,n}(u_{n*})$ is bounded below, we note that $T_{0,n} \geq -\|(z_n + \sigma^2) - (z_n + \sigma^2)\log(z_n + \sigma^2)\|_\infty$, which has a uniform bound for all n since $\|z_n - z\|_\infty \to 0$ and $z \in L^\infty(\Omega)$.

On the other hand, if $\|u_n\|_{BV} \to \infty$ and $J_0(v_n)$ is bounded, then $\|w_n\|_1 \to \infty$, in which case from (28) we have

$$T_{\alpha,n}(u_n) \geq C_2\|w_n\|_1 - M - \|z_n\|_\infty \log\left(C_2\|w_n\|_1 + M\right), \tag{32}$$

where M is the upper bound on $\|A_n\|_1 C_1 J_0(v_n) + (\gamma + \sigma^2)|\Omega|$ obtained using the uniform boundedness of both $\|A_n\|$ (Banach-Steinhaus) and $J_0(v_n)$. Since $\|z_n\|_\infty$ is uniformly bounded, (32) implies $T_{\alpha,n}(u_n) \to \infty$.

For condition 2, note that, using Jensen's inequality and the properties of the logarithm,

$$\begin{aligned}|T_{\alpha,n}(u) - T_\alpha(u)| = &\left| \int_\Omega \left((A_n - A)u - (z_n + \sigma^2) \log(A_n u + \gamma + \sigma^2) \right) dx \right. \\ &\left. + \int_\Omega \left((z + \sigma^2) \log(Au + \gamma + \sigma^2) \right) dx \right|, \\ \leq &\|A_n - A\|_1 \|u\|_1 + \|z_n - z\|_\infty \log(\|A_n\|_1 \|u\|_1 + (\gamma + \sigma^2)|\Omega|) \\ &+ \|z + \sigma^2\|_\infty \log \left\| (Au + \gamma + \sigma^2)/(A_n u + \gamma + \sigma^2) \right\|_1 .\end{aligned}$$

By assumption, $\|A_n - A\|_1, \|z_n - z\|_\infty \to 0$. Furthermore, by the Banach-Steinhaus Theorem, $\|A_n\|_1$ is uniformly bounded, and since we are assuming that $\|u\|_{BV}$ is bounded, by Lemma 1 we have that $\|u\|_1$ is bounded as well. Thus the first two terms on the right-hand side in (33) tend to zero as $n \to \infty$. For the third term note that

$$\left\| \frac{Au + \gamma + \sigma^2}{A_n u + \gamma + \sigma^2} - 1 \right\|_1 \leq \left\| \frac{1}{A_n u + \gamma + \sigma^2} \right\|_1 \|A_n - A\|_1 \|u\|_1,$$

which converges to zero since $\|1/(A_n u + \gamma + \sigma^2)\|_1$ is bounded and $\|A_n - A\|_1 \to 0$. Thus $\log(\|(Au + \gamma + \sigma^2)/(Au_n + \gamma + \sigma^2)\|_1) \to \log(1) = 0$, and hence

$$|T_{\alpha,n}(u) - T_\alpha(u)| \to 0. \tag{33}$$

This completes the proof. □

Corollaries 1 and 2 combine to give the following result.

Theorem 3 (Well-Posedness)**.** *Problem (13) is well-posed.*

2.3. Convergence of Minimizers

It remains to show that $\alpha > 0$ can be chosen so that, as $A_n \to A$ and $z_n \to z$, the solutions of (29) converge to the unique minimizer u_{exact} of the Poisson likelihood functional T_0 over $\mathcal{C}$. Let u_n be the solution, in argument, of

$$\min_{u \in \mathcal{C}} T_{\alpha_n,n}(u), \tag{34}$$

where $T_{\alpha_n,n}$ is defined in (29).

Theorem 4 (Convergence of Minimizers)**.** *Let $1 \leq p \leq d/(d-1)$. Suppose $\|z_n - z\|_\infty \to 0$, $A_n \to A$ pointwise in $L^p(\Omega)$ and $\alpha_n \to 0$ at a rate such that*

$$(T_{0,n}(u_{\text{exact}}) - T_{0,n}(u_{n*})))/\,\alpha_n \tag{35}$$

is bounded, where u_{exact} and u_{n*} are the unique minimizers of T_0 and $T_{0,n}$ respectively in $\mathcal{C}$. Then $u_n \to u_{\text{exact}}$ strongly in $L^p(\Omega)$ for $1 \leq p < d/(d-1)$ and weakly for $p = d/(d-1)$.

Proof. Again, due to (20), it suffices to consider the $\beta = 0$ case. Since u_n minimizes $T_{\alpha_n,n}$, we have

$$T_{\alpha_n,n}(u_n) \leq T_{\alpha_n,n}(u_{\text{exact}}). \tag{36}$$

Since $\{z_n\}$ and $\{A_n\}$ are uniformly bounded and $A_n \to A$ pointwise, $\{T_{\alpha_n,n}(u_{\text{exact}})\}$ is a bounded sequence, and (36) implies that $\{T_{\alpha_n,n}(u_n)\}$ is therefore also a bounded sequence.

Subtracting $T_{0,n}(u_{n*})$ from each term in (36), dividing by α_n, and using the decomposition $u_n = v_n + w_n$ yields

$$(T_{0,n}(u_n) - T_{0,n}(u_{n*}))/\,\alpha_n + J_0(v_n) \leq (T_{0,n}(u_{\text{exact}}) - T_{0,n}(u_{n*}))/\,\alpha_n + J_0(u_{\text{exact}}). \tag{37}$$

By (35), the right-hand side is bounded, implying the left hand side is bounded. Since $T_{0,n}(u_n) - T_{0,n}(u_{n*})$ is nonnegative, $J_0(v_n)$ is therefore also bounded. The boundedness of $T_{\alpha_n,n}(u_n)$ together with (32) imply that $\|w_n\|_1$ is bounded. The BV-boundedness of $\{u_n\}$ then follows immediately from (25).

We show that $u_n \to u_{\text{exact}}$ (weakly for $p = d/(d-1)$) by showing that every subsequence of $\{u_n\}$ contains a subsequence that converges to u_{exact}. Every subsequence $\{u_{n_j}\}$ of $\{u_n\}$ is BV-bounded - since $\{u_n\}$ is - and, by Lemma 1, has a convergent subsequence. Therefore, without loss of generality, we can assume that $\{u_{n_j}\}$ converges strongly (weakly for $p = d/(d-1)$) to some $\hat{u} \in L^p(\Omega)$. Then

$$\begin{aligned} T_0(\hat{u}) \;=\; & \int_\Omega (A(\hat{u} - u_{n_j}) + (A - A_{n_j})u_{n_j} + (z_{n_j} - z)\log(A\hat{u} + \gamma + \sigma^2))\,dx \\ & - \int_\Omega (z_{n_j} + \sigma^2)\log((A_{n_j}u_{n_j} + \gamma + \sigma^2)/(A\hat{u} + \gamma + \sigma^2))\,dx + T_{0,n_j}(u_{n_j}), \end{aligned}$$

which, as in previous arguments, yields

$$\begin{aligned} |T_{0,n_j}(u_{n_j}) - T_0(\hat{u})| \leq & \int_\Omega A\left(\hat{u} - u_{n_j}\right)\,dx + \|z_{n_j} - z\|_\infty \log(\|A\|_1\|\hat{u}\|_1 + \gamma|\Omega|) \\ & + \|z_{n_j} + \sigma^2\|_\infty \log\|(A_{n_j}u_{n_j} + \gamma + \sigma^2)/(A\hat{u} + \gamma + \sigma^2)\|_1 \\ & + \|A - A_{n_j}\|_1\|u_{n_j}\|_1. \end{aligned}$$

Then for $1 \leq p \leq d/d-1$,

$$\|z_{n_j} - z\|_\infty \log(\|A\|_1\|\hat{u}\|_1 + (\gamma + \sigma^2)|\Omega|) \to 0,$$

since $\|z_{n_j} - z\|_\infty \to 0$ and $\log(\|A\|_1\|\hat{u}\|_1 + (\gamma + \sigma^2)|\Omega|)$ is constant, and

$$\|A - A_{n_j}\|_1\|u_{n_j}\|_1 \to 0$$

since $\|A - A_{n_j}\|_1 \to 0$ and $\|u_{n_j}\|_1$ is uniformly bounded.

Since A is a bounded linear operator and Ω is a set of finite measure, $F(u) = \int_\Omega Au\,dx$ is a bounded linear functional on $L^p(\Omega)$. The weak convergence of $\{u_{n_j}\}$ (recall that strong convergence implies weak convergence) then implies $\int_\Omega Au_{n_j}\,dx \to \int_\Omega A\hat{u}\,dx$, which yields $\int_\Omega A\left(\hat{u} - u_{n_j}\right)\,dx \to 0$.

Since A is compact, it is completely continuous, i.e. the weak convergence of u_{n_j} to $\hat{u}$ implies that $\|Au_{n_j} - A\hat{u}\|_1 \to 0$ (cf. [4, Prop. 3.3]). Thus, since $\left\|\frac{1}{A\hat{u}+\gamma+\sigma^2}\right\|_1$ is bounded, and

$$\begin{aligned}\left\|\frac{A_{n_j}u_{n_j}+\gamma+\sigma^2}{A\hat{u}+\gamma+\sigma^2}-1\right\|_1 &\leq \left\|\frac{1}{A\hat{u}+\gamma+\sigma^2}\right\|_1 \|A_{n_j}u_{n_j}-A\hat{u}\|_1,\\ &\leq \left\|\frac{1}{A\hat{u}+\gamma+\sigma^2}\right\|_1 \left(\left\|A_{n_j}-A\right\|_1 \|u_{n_j}\|_1 + \|Au_{n_j}-A\hat{u}\|_1\right)\end{aligned}$$

we have that $\|z_{n_j}\|_\infty \log\|(A_{n_j}u_{n_j}+\gamma+\sigma^2)/(A\hat{u}+\gamma+\sigma^2)\|_1 \to 0$. Therefore

$$T_0(\hat{u}) = \lim_{n_j\to\infty} T_{0,n_j}(u_{n_j}).$$

Invoking (37), (35), and (33), respectively, yields

$$\lim_{n_j\to\infty} T_{0,n_j}(u_{n_j}) = \lim_{n_j\to\infty} T_{0,n_j}(u_{n_j*}) = \lim_{n_j\to\infty} T_{0,n_j}(u_{\text{exact}}) = T_0(u_{\text{exact}}),$$

so $T_0(\hat{u}) = T_0(u_{\text{exact}})$. Since u_{exact} is the unique minimizer of T_0, $\hat{u} = u_{\text{exact}}$. Therefore $\{u_{n_j}\}$ converges strongly (weakly for $p = d/(d-1)$) to u_{exact} in $L^p(\Omega)$. This completes the proof. □

3. Numerical Experiments

In this section, we present numerical experiments to demonstrate that total variation-penalized Poisson likelihood estimation can be effective in practice. To do this, we consider a data set generated using the statistical model in (7) with $n = 256$. The blurring matrix $\mathbf{A}$ that was used was generated using the physical model for atmospheric blurring discussed in [11, Chapter 5]. The piecewise constant, true image $\mathbf{u}_{\text{true}}$ is the rendition of a satellite given on the left in Figure 1. The readout noise variance σ^2 was taken to be 25, and the Poisson background count parameter γ was taken to be 10, which are physically realistic values for these parameters. To generate Poisson noise, the `poissrnd` function in MATLAB's Statistics Toolbox was used. The corresponding blurred, noisy data $\mathbf{z}$ is given on the right hand side in Figure 1. The data generation code was a modified version of the two-dimensional data generation code from [11].

With the blurred, noisy data in hand, we estimate $\mathbf{u}_{\text{true}}$ by approximately solving (12) using a nonnegatively contrained iterative method. The total variation smoothing parameter β was taken to be 1.

3.1. Preliminaries

We first present some preliminary definitions and formulas. The gradient and Hessian of $T_\alpha(\mathbf{u})$, as defined in (12), are given by

$$\begin{aligned}\nabla T_\alpha(\mathbf{u}) &= \nabla T_0(\mathbf{u}) + \alpha\nabla J_\beta(\mathbf{u}),\\ \nabla^2 T_\alpha(\mathbf{u}) &= \nabla^2 T_0(\mathbf{u}) + \alpha\nabla^2 J_\beta(\mathbf{u}).\end{aligned}$$

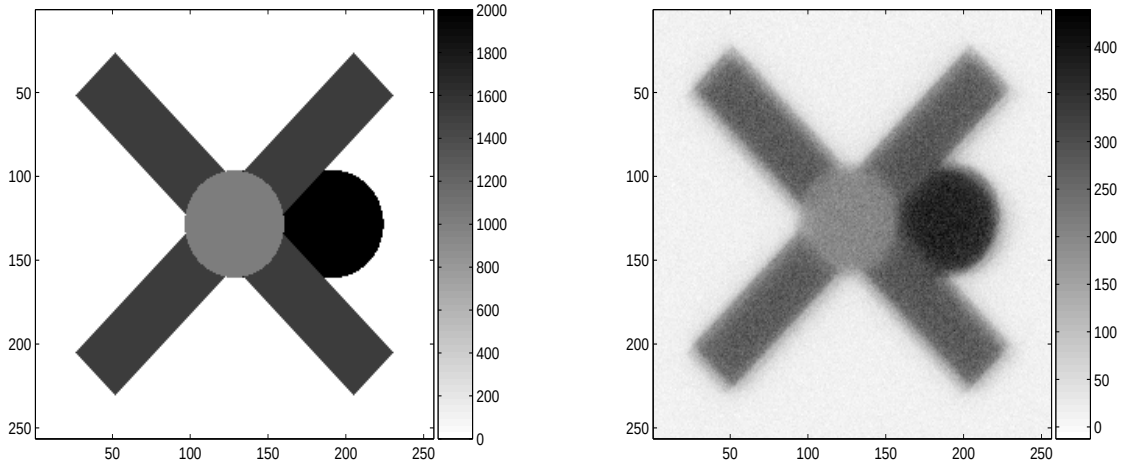

Figure 1. *Object and Blurred, Noisy Image. On the left is the true object* $\mathbf{u}_{\text{true}}$*. On the right, is the blurred, noisy image* $\mathbf{z}$*.*

The gradient and Hessian of the Poisson likelihood functional $T_0(\mathbf{u})$ have expressions

$$\nabla T_0(\mathbf{u}) = \mathbf{A}^T \left(\frac{\mathbf{A}\mathbf{u} - (\mathbf{z} - \gamma)}{\mathbf{A}\mathbf{u} + \gamma + \sigma^2} \right), \tag{38}$$

$$\nabla^2 T_0(\mathbf{u}) = \mathbf{A}^T \left(\frac{\mathbf{z} + \sigma^2}{(\mathbf{A}\mathbf{u} + \gamma + \sigma^2)^2} \right) \mathbf{A}. \tag{39}$$

Note the similarities with (17) and (18). Multiplication and division of vectors is done component-wise.

The gradient and Hessian of $J_\beta(\mathbf{u})$ require a bit more work. First, recall from (4) that in two-dimensions

$$J_\beta(u) = \int_\Omega \sqrt{\left(\frac{\partial u}{\partial x}\right)^2 + \left(\frac{\partial u}{\partial y}\right)^2 + \beta}\, dxdy, \tag{40}$$

and the discrete analogue is given by

$$J_\beta(\mathbf{u}) = \Delta x \Delta y \sum_{i=1}^{n} \sum_{i=1}^{n} \sqrt{(D_x\mathbf{u})^2 + (D_y\mathbf{u})^2 + \beta}, \tag{41}$$

where D_x and D_y are the $n^2 \times n^2$ matrices corresponding to the grid approximations of the first derivative with respect to x and y respectively, and $(D_x\mathbf{u})^2$ and $(D_y\mathbf{u})^2$ denote the vectors whose elements are the component-wise squares of the elements of $D_x\mathbf{u}$ and $D_y\mathbf{u}$, respectively. In our computations, Ω was taken to be the unit square and so $\Delta x = \Delta y = \frac{1}{n}$.

The gradient and Hessian of J_β are given by its first and second Gateaux derivatives, which are given by

$$\begin{aligned} \nabla J_\beta(\mathbf{u}) &= \frac{2}{n^2} L_1(\mathbf{u})\mathbf{u}, \\ \nabla^2 J_\beta(\mathbf{u}) &= \frac{2}{n^2} L_1(\mathbf{u}) + \frac{4}{n^2} L_2(\mathbf{u}), \end{aligned} \tag{42}$$

where, if $\psi(t) \stackrel{\text{def}}{=} \sqrt{t+\beta}$ and $D\mathbf{u}^2 \stackrel{\text{def}}{=} (D_x\mathbf{u})^2 + (D_y\mathbf{u})^2$,

$$L_1(\mathbf{u}) = [D_x^T D_y^T] \begin{bmatrix} \text{diag}(\psi'(D\mathbf{u}^2)) & \mathbf{0} \\ \mathbf{0} & \text{diag}(\psi'(D\mathbf{u}^2)) \end{bmatrix} \begin{bmatrix} D_x \\ D_y \end{bmatrix}, \tag{43}$$

$$L_2(\mathbf{u}) = [D_x^T D_y^T] \begin{bmatrix} \text{diag}((D_x\mathbf{u})^2\psi''(D\mathbf{u}^2)) & \text{diag}((D_x\mathbf{u})(D_y\mathbf{u})\psi''(D\mathbf{u}^2)) \\ \text{diag}((D_x\mathbf{u})(D_y\mathbf{u})\psi''(D\mathbf{u}^2)) & \text{diag}((D_x\mathbf{u})^2\psi''(D\mathbf{u}^2)) \end{bmatrix} \begin{bmatrix} D_x \\ D_y \end{bmatrix}.$$

Here multiplication of vectors is done component-wise, and $\text{diag}(\mathbf{v})$, where $\mathbf{v}$ is $n^2 \times 1$, is the $n^2 \times n^2$ diagonal matrix with $\mathbf{v}$ as its diagonal. For a more detailed treatment of these computations see [11, Chapter 8].

The nonnegatively constrained methods that we will present require some additional notation and definitions. We will use $\mathbf{u} \geq \mathbf{0}$ to denote component-wise nonnegativity for $\mathbf{u}$. The *active set* for $\mathbf{u} \geq \mathbf{0}$ is defined

$$\mathcal{A}(\mathbf{u}) = \{i \mid u_i = 0\}.$$

The complementary set of indices is called the *inactive set* and is denoted by $\mathcal{I}(\mathbf{u})$. The orthogonal projection of a vector $\mathbf{u} \in \mathbb{R}^{n^2}$ onto $\{\mathbf{x} \in \mathbb{R}^{n^2} \mid \mathbf{x} \geq \mathbf{0}\}$ is given by

$$P(\mathbf{u}) = \max(\mathbf{u}, \mathbf{0}),$$

where the maximum is computed component-wise. Finally, let $D_{\mathcal{I}}(\mathbf{u})$ denote the diagonal matrix with components

$$[D_{\mathcal{I}}(\mathbf{u})]_{ii} = \begin{cases} 1, & i \in \mathcal{I}(\mathbf{u}) \\ 0, & i \in \mathcal{A}(\mathbf{u}). \end{cases} \tag{44}$$

Then $D_{\mathcal{A}}(\mathbf{u}) \stackrel{\text{def}}{=} I - D_{\mathcal{I}}(\mathbf{u})$, where I is the $n^2 \times n^2$ identity matrix.

3.2. Nonnegatively Constrained Minimization Methods

Here we present two computational methods for approximately solving (12). We begin with the *projected gradient method*, which is one of the simplest methods for nonnegatively constrained minimization. In principle, projected gradient generates a sequence of approximate solutions $\{\mathbf{u}_k \mid \mathbf{u}_k \geq \mathbf{0}\}$ of problem (12) via the following iteration:

$$\mathbf{v}_k = -\nabla T_\alpha(\mathbf{u}_k); \tag{45}$$

$$\lambda_k = \arg\min_{\lambda > 0} T_\alpha(P(\mathbf{u}_k + \lambda \mathbf{v}_k)); \tag{46}$$

$$\mathbf{u}_{k+1} = P(\mathbf{u}_k + \lambda_k \mathbf{v}_k). \tag{47}$$

In practice, subproblem (46) is only approximately solved. For our experiments a projected, quadratic line search algorithm was used. In order to ensure that the algorithm has satisfactory convergence properties, λ was chosen to satisfy the Wolfe conditions,

$$\phi(\lambda) \leq \phi(0) + c_1 \tau \phi'(0), \tag{48}$$

$$\phi'(\lambda) \geq c_2 \phi'(0), \tag{49}$$

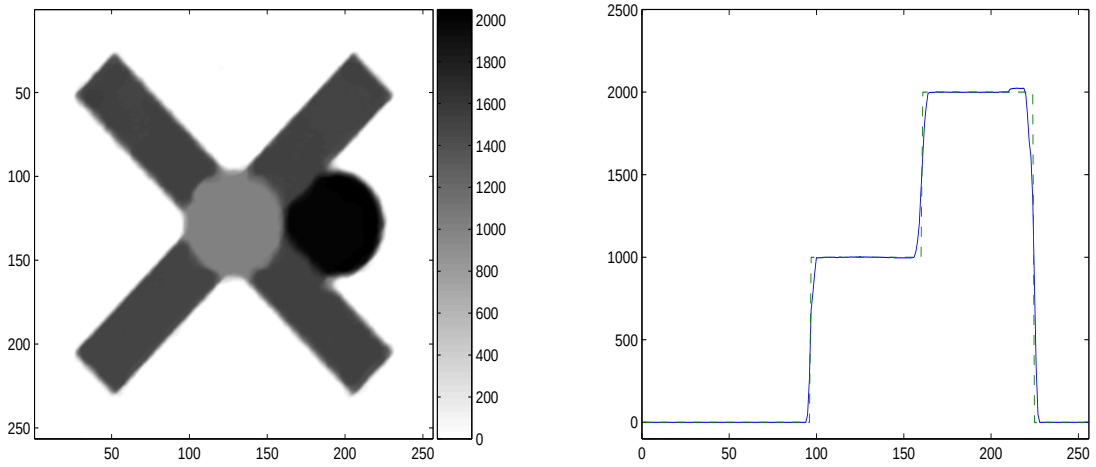

Figure 2. *Object Reconstruction. On the left is a plot of the reconstruction. On the right is a cross section of both the reconstruction (solid line) and the true image (dashed line) corresponding to the 128th row.*

where $\lambda > 0$, and $\phi(\lambda) = T_\alpha(\mathbf{u}_k + \lambda \mathbf{v}_k)$. For a more detailed description of such an algorithm see [7].

Due to the fact that the optimization problem is constrained, large scale and highly ill-conditioned, a more robust method than projected gradient is needed to obtain approximate solutions of (12) sufficiently near to the exact solution. Such a method results if (45) is replaced by

$$\mathbf{v}_k = -[D_{\mathcal{I}}(\mathbf{u}_k)\mathbf{B}(\mathbf{u}_k)D_{\mathcal{I}}(\mathbf{u}_k) + D_{\mathcal{A}}(\mathbf{u}_k)]^{-1}\nabla T_\alpha(\mathbf{u}_k), \tag{50}$$

where

$$\mathbf{B}(\mathbf{u}_k) = \nabla^2 T_0(\mathbf{u}_k) + \alpha \frac{2}{n^2} L_1(\mathbf{u}_k). \tag{51}$$

Here $L_1(\mathbf{u}_k)$ is defined in (43). If the $\frac{4}{n^2}L_2(\mathbf{u}_k)$ term in (42) is included in (51), the resulting algorithm, (50), (46), (47), is known as the projected Newton method [3, 6]. However, we chose to drop this term because the resulting algorithm is more effective and robust. For our test problem, we compute an approximation of (50) using the conjugate gradient iteration with a maximum number of iterations equal to 1000. As in the projected gradient method, a projected, quadratic line search algorithm was used in order to ensure that the method has satisfactory convergence properties.

In order to obtain sufficiently accurate solutions of (12) in a computationally efficient manner, we used 30 iterations of projected gradient to obtain a good initial guess for the quasi-Newton iterations. We then computed 70 iterations of the quasi-Newton method to obtain the reconstruction on the left in Figure 2. In all iterations, the regularization parameter $\alpha = 1$ was used. The reconstruction is accurate in appearance, and the cross section included on the right in Figure 2 indicates that both total variation regularization as well as the nonnegativity constraints are effective.

Note that if the nonnegativity constraint is dropped, the Poisson likelihood is replaced by the least squares likelihood in the definition of T_α, and λ is taken to be 1 at every iteration, then (50), (46), (47) becomes

$$\mathbf{u}_{k+1} = \mathbf{u}_k - [\mathbf{A}^T\mathbf{A} + \alpha\frac{2}{n^2}L_1(\mathbf{u}_k)]^{-1}\nabla T_\alpha(\mathbf{u}_k), \tag{52}$$

which is the lagged diffusivity fixed point iteration of [12]. Thus, the nonnegatively constrained quasi-Newton method presented above, can be viewed as the analogue of the lagged diffusivity fixed point iteration for total variation penalized, nonnegatively constrained Poisson likelihood estimation.

4. Conclusions

In image deblurring problems, the collected data is a realization of a random vector whose components are, in many cases, accurately modeled by a Poisson distribution. The least squares approach is commonly used nonetheless, due in large part to the facts that the resulting methods are straightforward to implement and that regularization in conjunction with least squares data fitting has been extensively studied and stands on firm theoretical footings. Similar theoretical foundations must be developed for regularization approaches in which the fit-to-data functional is not of least squares type. In this paper, we have considered the Poisson likelihood fit-to-data functional in conjunction with total variation regularization. The *a priori* knowledge of the nonnegativity of the true image is incorporated into the corresponding variational (constrained minimization) problem (13). We proved that (13) is well-posed and that as errors in the data z and in the operator A disappear, the regularization parameter α can be chosen so that the corresponding minimizers converge to the unique minimizer of T_0 over $\mathcal{C}$.

We verified the practical validity of total variation-penalized Poisson likelihood estimation by implementing the approach numerically. This required an accurate approximate solution of the nonnegatively constrained minimization problem (12). For this, the standard gradient projection method was used in conjunction with a projected quasi-Newton method introduced in this paper, and the numerical results presented here clearly demonstrate the effectiveness of the approach. Future analysis will include the development of a more complete computational paradigm for the solution of this problem.

5. References

[1] R. Acar and C.R. Vogel, *Analysis of bounded variation penalty methods for ill-posed problems*, Inverse Problems, 10 (1994), pp. 1217-1229.

[2] T. Asaki, R. Chartrand and T. Le, *A Variational Approach to Reconstructing Images Corrupted by Poisson Noise*, UCLA CAM Report 05-49, November 2005.

[3] D. P. Bertsekas, *Projected Newton Methods for Optimization Problems with Simple Constraints*, SIAM Journal on Control and Optimization, **20** (1982), pp. 221–246.

[4] John B. Conway, *A Course in Functional Analysis*, Second Edition, Springer, 1990.

[5] W. Feller, *An Introduction to Probability Theory and Its Applications*, Wiley, New York, 1971.

[6] C. T. Kelley, *Iterative Methods for Optimization*, SIAM, Philadelphia, 1999.

[7] J. Nocedal and S. Wright, *Numerical Optimization*, Springer 1999.

[8] D. L. Snyder, A. M. Hammoud, and R. L. White, *Image recovery from data acquired with a charge-coupled-device camera*, Journal of the Optical Society of America A, **10** (1993), pp. 1014–1023.

[9] D. L. Snyder, C. W. Helstrom, A. D. Lanterman, M. Faisal, and R. L. White, *Compensation for readout noise in CCD images*, Journal of the Optical Society of America A, **12** (1995), pp. 272–283.

[10] A. N. Tikhonov, A. V. Goncharsky, V. V. Stepanov and A. G. Yagola, *Numerical Methods for the Solution of Ill-Posed Problems*, Kluwer Academic Publishers, 1990.

[11] C. R. Vogel, *Computational Methods for Inverse Problems*, SIAM, Philadelphia, 2002.

[12] C. R. Vogel and M. E. Oman, *A fast, robust algorithm for total variation based reconstruction of noisy, blurred images*, IEEE Transactions on Image Processing, **7** (1998), pp. 813-824.

[13] E. Zeidler, *Applied Functional Analysis: Main Principles and their Applications*, Springer-Verlag, New York, 1995.